JACS
JOURNAL OF THE AMERICAN CHEMICAL SOCIETY
Article
pubs.acs.org/JACS

Cationic Covalent Organic Frameworks: A Simple Platform of Anionic Exchange for Porosity Tuning and Proton Conduction

Heping Ma,[†] Bailing Liu,[‡] Bin Li,*[,†] Liming Zhang,[†] Yang-Guang Li,[‡] Hua-Qiao Tan,[‡] Hong-Ying Zang,*[,‡] and Guangshan Zhu[‡]

[†]State Key Laboratory of Luminescence and Applications, Changchun Institute of Optics Fine Mechanics and Physics, Chinese Academy of Sciences, Changchun 130033, P. R. China

[‡]Key Lab of Polyoxometalate Science of Ministry of Education, Faculty of Chemistry, Northeast Normal University, Changchun 130024, P. R. China

Supporting Information

ABSTRACT: Mimicking proton conduction mechanism of Nafion to construct novel proton-conducting materials with low cost and high proton conductivity is of wide interest. Herein, we have designed and synthesized a cationic covalent organic framework with high thermal and chemical stability by combining a cationic monomer, ethidium bromide (EB) (3,8-diamino-5-ethyl-6-phenylphenanthridinium bromide), with 1,3,5-triformylphloroglucinol (TFP) in Schiff base reactions. This is the first time that the stable cationic crystalline frameworks allowed for the fabrication of a series of charged COFs (**EB-COF:X, X = F, Cl, Br, I**) through ion exchange processes. Exchange of the extra framework ions can finely modulate the COFs' porosity and pore sizes at nanoscale. More importantly, by introducing $PW_{12}O_{40}^{3-}$ into this porous cationic framework, we can greatly enhance the proton conductivity of ionic COF-based material. To the best of our knowledge, **EB-COF:PW_{12}** shows the best proton conductivity at room temperature among ever reported porous organic materials.

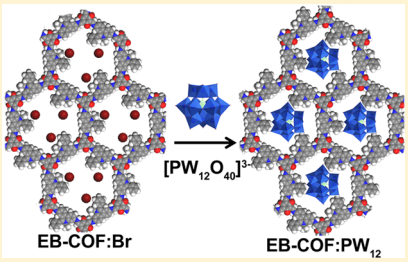

INTRODUCTION

Covalent organic frameworks (COFs) are an emerging class of porous crystalline polymers with highly ordered organic building blocks and well-defined nanopores.[1−6] COFs have shown excellent performance in gas adsorption and storage,[7,8] heterogeneous catalysis,[9−12] optoelectronics,[13−17] energy storage,[18,19] and sensors[20] because of their structural regularity and monodisperse pore size. A major goal in COFs is to tailor the shape, size, and chemical nature of pores.[21−25] One approach to alter COF's pore structure is to change the geometry of diverse monomers during the synthesis. Although variation of the monomer results in COFs with different pore sizes, the structural changes of COFs are often inconsistent because of the changes in the fundamental geometry of the core framework.[26] Another feasible method to tune the pore size while preserving the architecture is ion exchange, which is a well-known feature of zeolites. Although a few ionic amorphous porous organic materials with ion exchange properties exhibit promising applications in gas separation and catalysis,[27−31] it is still a challenge for crystalline COFs as a platform for ion exchange due to the neutral nature of COF frameworks. Constructing sufficiently stable charged COFs would open a door for these well-defined crystalline porous networks for a wide variety of applications, for example, as ion exchangers, ion conductors, solid electrolytes, and solid catalysts.

Research on proton-conducting materials sparked tremendous interest due to urgent demand in fuel cells and electronic devices.[32,33] Commercially available Nafion films limit wide applications because of their high cost and deactivation above 80 °C, which forces exploration of new proton-conducting materials. Recently, metal−organic frameworks (MOFs)/porous coordination polymers (PCPs) show possibilities as candidates for proton-conducting application.[34] Polyoxometalates (POMs) are a type of nanosized clusters with diverse architectures being studied extensively for potential applications in catalysis, electronic devices, and fuel cells.[35,36] However, the high solubility of POMs in a polar reagent hinders their development in fuel cells.[37,38] Two approaches have been employed to overcome this defect: one is to load POMs onto high surface materials, and another is to substitute H^+ for large cations such as Rb^+, Cs^+, and NH_4^+.[32] We supposed that a combination of the two approaches using porous cationic covalent organic frameworks, i.e., "killing two birds with one stone" would be an efficient methodology.

Herein, we hypothesized that a stable porous cationic organic framework might be able to load polyoxometalate anions so as to form novel proton-conducting materials. We designed and synthesized the first cationic COF, termed **EB-COF:Br**, possessing positively charged open frameworks with Br^- as counterions (Scheme 1). Then, the chemically stable and porous **EB-COF:X** (X = F, Cl, Br, I, $PW_{12}O_{40}^{3-}$) were investigated after ion exchange processes. More importantly, we measured the proton conductivity of the **EB-COF:Br** and **EB-COF:PW_{12}** ($PW_{12}O_{40}^{3-}$ is abbreviated as PW_{12}) to investigate

Received: December 27, 2015
Published: April 19, 2016

DOI: 10.1021/jacs.5b13490
J. Am. Chem. Soc. 2016, 138, 5897−5903

Scheme 1. (a) Schematic Representation of the Synthesis of EB-COF:Br: (b) Top Views and (c) Side Views of the Offset AA Stacking Structure of the EB-COF:Br

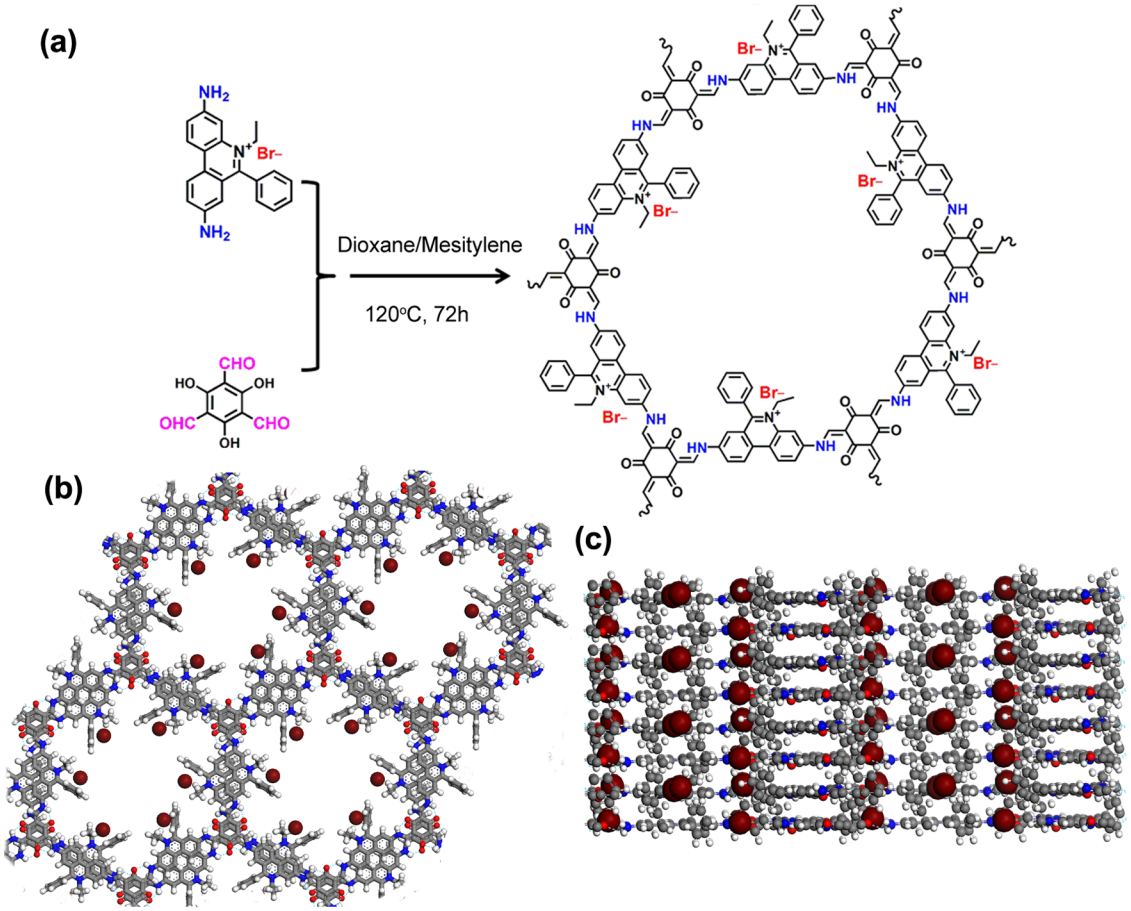

the polyoxometalate effect on the proton conductivity of cationic COF.

EXPERIMENTAL SECTION

Synthesis of EB-COF:Br. In the typical synthesis, a pyrex tube (10 × 8 mm^2 and length 18 cm) is charged with 1,3,5-triformylphloroglucinol (TFP) (0.2 mmol), ethidium bromide (EB) (0.3 mmol), 2 mL of 1,4-dioxane−mesitylene (v/v, 1:1), and 0.2 mL of 6 M aqueous acetic acid. The tube was then flash frozen at 77 K (liquid N_2 bath) and degassed by freeze−pump−thaw cycles. The tube was sealed off and then heated at 120 °C for 3 days. After that, we turned off the oven, and the cooling process was implementing undisturbed. A dark red precipitate was collected by filtration and washed with THF. The powder collected was then Soxhlet extracted with THF and methanol and dried at 100 °C under vacuum for 12 h to get the corresponding COFs in ∼85% isolated yield.

Synthesis of EB-COF:F, EB-COF:Cl, and EB-COF:I. Activated EB-COF:Br (1.5 g) was dispersed in 15 mL of a 1:1 H_2O/methanol saturated solution of corresponding halide salts (sodium fluoride, sodium chloride, or potassium iodide). After the mixture was stirred for 24 h, the residue was filtered. The above step was repeated four times, and the precipitate was washed with H_2O (20 mL) five times, which then afforded the goal product.

Other experiment and characterization details are in the Supporting Information.

RESULTS AND DISCUSSIONS

The IR spectra of **EB-COF:Br** and the initial monomers are shown in Figure S1a. The disappearance of characteristic absorption peaks of the N—H stretching bands of EB (3185, 3309 cm^{-1}) and the aldehyde group stretching bands of TFP (C═O at 1643 cm^{-1}, O═C—H at 2889 cm^{-1}) provides direct evidence for the completion of co-condensation reaction. Both the lack of OH and imine (C═N) stretches and the rise of a strong peak at 1593 cm^{-1} resulting from the C═C stretching in the FT-IR spectra (Figure S1b) demonstrate that the COF exists in the keto form.[39]

The **EB-COF:Br** in the keto form was also unambiguously confirmed by ^{13}C MAS solid-state nuclear magnetic resonance (NMR) spectrum (Figure S2). An NMR signal around 167.2 ppm is observed, which is assigned to the carbon atom in the C═C groups. The well-resolved peak is detected at 47.1 and 18.2 ppm associated with the ethyl carbon atom in EB, indicating that ethidium bromide is retained in **EB-COF:Br**. The distinct NMR shifts assigned to the benzene rings in the range 130−150 ppm occur, which indicates that the **EB-COF:Br** framework is composed of highly conjugated phenyl groups. Scanning electron microscopy (SEM) images show that **EB-COF:Br** has a spherical morphology, with dimensions ranging from 200 to 500 nm (Figure S3).

Powder X-ray diffraction (PXRD) was used to investigate the crystallinity of the **EB-COF:Br** sample. As observed in Figure 1a, the as-synthesized COF displays strong diffraction peaks with low signal-to-noise ratios, indicative of the high crystallinity of **EB-COF:Br**. The **EB-COF:Br** exhibits an intense diffraction peak at 3.3° and a broad peak at 27°, corresponding to the 100 and 001 reflections, respectively. The chemical stability of the keto form COF is remarkable because

DOI: 10.1021/jacs.5b13490
J. Am. Chem. Soc. 2016, 138, 5897−5903

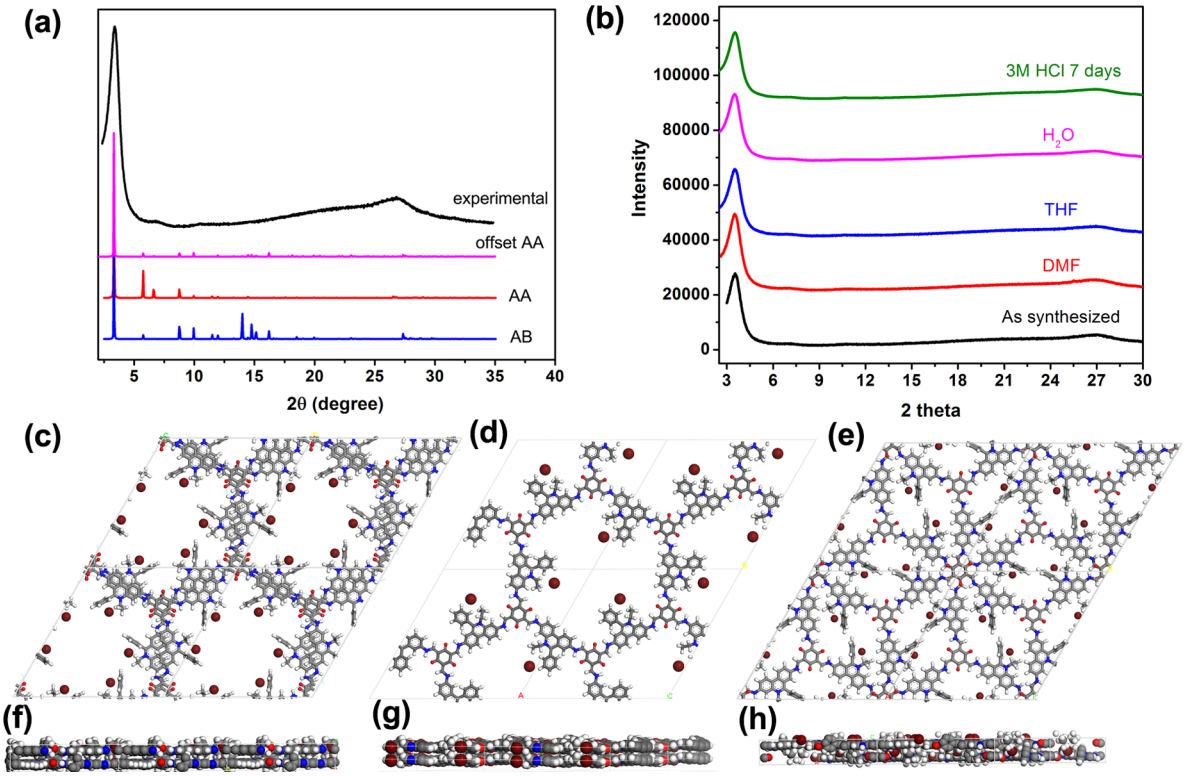

Figure 1. (a) Experimental PXRD data of as-prepared COF (black) vs simulated patterns for the 1.2 Å offset AA (pink), ideal AA (red), and staggered AB (blue) arrangements of the 2D layer. (b) XRD patterns of **EB-COF:Br** upon treatment in different conditions. Top view of (c) 1.2 Å offset AA structure, (d) ideal AA structure, and (e) ideal staggered AB structure. Side view of (f) offset AA structure, (g) ideal AA structure, and (h) ideal AB structure.

it retains the crystalline framework after immersion in organic solvents and even in 3 M HCl aqueous solution (Figure 1b). Structural resolution based on X-ray diffraction measurement in conjunction with structural simulation indicates that **EB-COF:Br** is a typical 2D layered hexagonal network. The alignment of layers is addressed by building up the monolayer structure and then constructs layered structures via energy optimization.[25] After the geometrical energy minimization using the universal force-field implemented in the forcite module, **EB-COF** in the offset of 1.2 Å between the AA stacking layers has significantly lower total energy (285.98 kcal/mol) compared to the values calculated for ideal AA and AB stacking models (531.91 and 451.25 kcal/mol for AA and AB stacking, respectively), indicating the offset AA stacking is more energetically favored (Figures S4–S6). The low total energy of the offset AA stacking model may benefit from the slight slip between layers avoiding cationic pyridinium centers directly on top of each other. In the simulated PXRD of the offset AA stacking mode, the 100 diffraction peak exhibits the strongest diffraction intensity, which is in agreement with experimental results (Figure 1a). In addition to the (100) peaks, diffraction peaks assigned to other facets show much lower diffraction intensity compared with that in ideal AA or AB stacking. Together with low total energy of the offset AA stacking mode, we propose that the preferred structure of **EB-COF** is a 2D layered hexagonal network consisting of AA stacking structures with 1.2 Å offset between the layers.

We conducted ion exchange experiments of **EB-COF:Br** and chose halide ions (F^-, Cl^-, and I^-) to assess the ion exchange properties of **EB-COF:Br**. The exchange of the extra framework anion with F^-, Cl^-, or I^- ions was carried out at room temperature. In ion exchange processes, the corresponding alkali halide was added into the suspension of **EB-COF:Br** in the 1:1 water–methanol solution. After the ion exchange process completion, the precipitates were filtered, thoroughly washed with water, and dried at 120 °C under vacuum to give **EB-COF:F**, **EB-COF:Cl**, and **EB-COF:I**, respectively. The unchanged PXRD patterns confirmed structural maintenance of the COF frameworks after ion exchange experiments (Figure S7).

EDS and XPS were performed to demonstrate the completion of the halide ions during the exchanging process. The high-resolution XPS analyses of halide ions in **EB-COF** indicate that halogen is present in the ionic state (Figure S8–S11).[40] EDS results show that the signal from Br is very low and the corresponding signals from F, Cl, and I are detected in **EB-COF:F**, **EB-COF:Cl**, and **EB-COF:I**, respectively, which means the Br ion is well-exchanged by another halide (Figure S12). The degree of halide ions exchange is demonstrated by an ion-chromatographic analyzer. As shown in Table S1, Br^- ions are almost completely substituted by other halide ions, affording the corresponding **EB-COF:F**, **EB-COF:Cl**, and **EB-COF:I** products. The thermogravimetric analysis (TGA) shows that the decomposition of **EB-COFs** starts in the range 300–400 °C in air, suggesting these materials possess excellent thermal stability (Figure S13).

Changes of the porosity and pore sizes after ion exchange of **EB-COFs** were investigated by nitrogen adsorption measurement at 77 K. As shown in Figure 2, a sharp increase in gas uptake is observed at low pressure in the nitrogen adsorption–desorption isotherms of all **EB-COFs**, which indicates that all COFs are microporous networks. The Brunauer–Emmett–

DOI: 10.1021/jacs.5b13490
J. Am. Chem. Soc. 2016, 138, 5897–5903

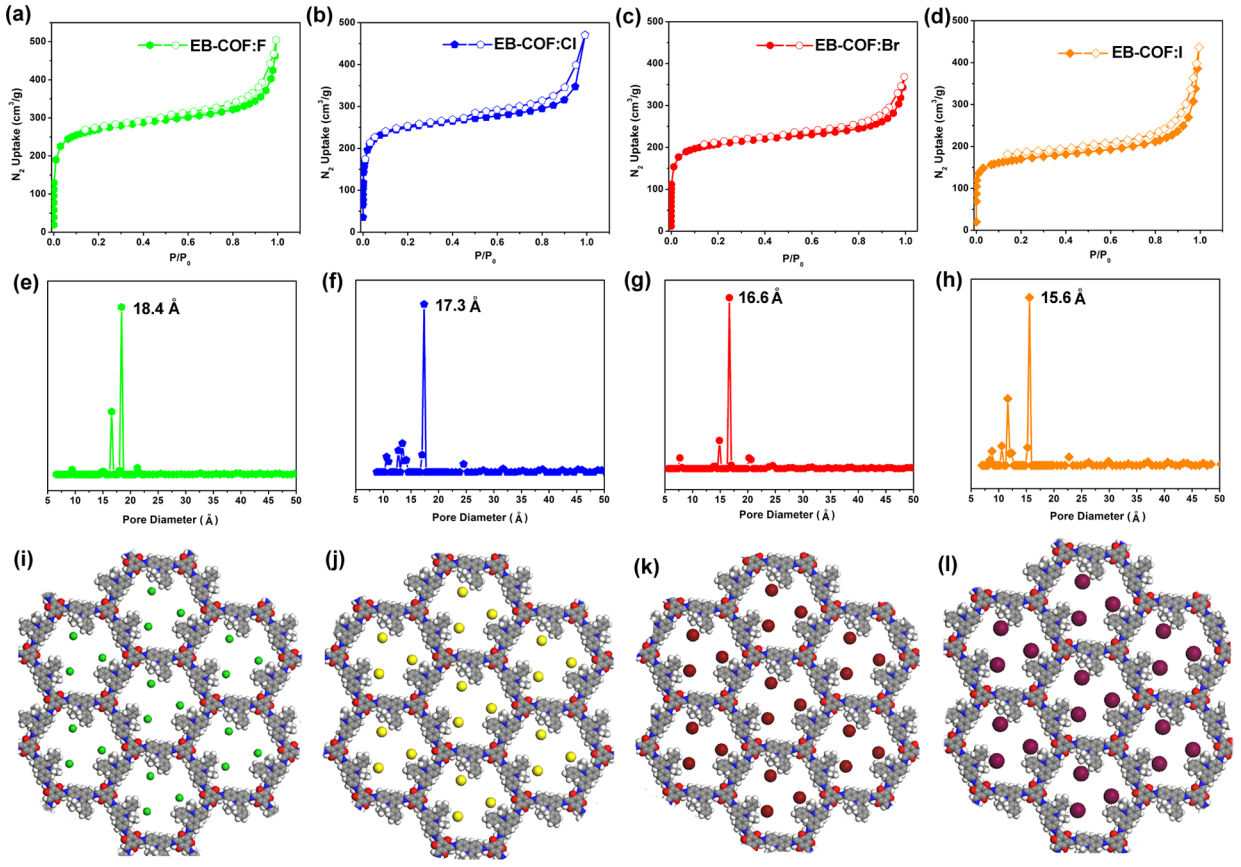

Figure 2. (a–d) Nitrogen sorption isotherms for (a) **EB-COF:F**, (b) **EB-COF:Cl**, (c) **EB-COF:Br**, and (d) **EB-COF:I** at 77 K. (e–h) Pore size distribution of (e) **EB-COF:F**, (f) **EB-COF:Cl**, (g) **EB-COF:Br**, and (h) **EB-COF:I**. (i–l) One layer extended structure of (i) **EB-COF:F**, (j) **EB-COF:Cl**, (k) **EB-COF:Br**, and (l) **EB-COF:I**. C, gray; H, white; N, blue; O, red; F, green; Cl, yellow; Br, dark red; I, maroon.

Teller (BET) surface area of **EB-COF:F** is measured as 1002 m^2/g. The BET surface area is decreasing with the increase of halide atomic weights from Cl to I. **EB-COF:Cl** has a BET surface area of 954 m^2/g, while BET surface areas are decreased to 774 and 616 m^2/g for **EB-COF:Br** and **EB-COF:I**, respectively. The pore size distributions (PSDs) of **EB-COFs** are demonstrated by the nonlocal density functional theory (NLDFT) based on the model N_2 at 77 K on carbon (cylindrical pores). The pore size of **EB-COF:Br** is 16.6 Å, which coincides with the theoretical pore size of the simulated structure. The PSD of **EB-COF:F** and **EB-COF:Cl** exhibits dominant ones of about 18.4 and 17.3 Å, while the PSD of **EB-COF:I** exhibits a dominant pore diameter of 15.6 Å. The decreasing trend in the pore sizes of **EB-COF:F**, **EB-COF:Cl**, **EB-COF:Br**, and **EB-COF:I** samples can be explained by the increased ionic radius of F^- (2.66 Å), Cl^- (3.62 Å), Br^- (3.92 Å), and I^- (4.40 Å). The results demonstrate that the pore size of **EB-COF** can be finely controlled by facile anionic-exchange processes. Furthermore, we exchanged the **EB-COF:Br** with larger POM anions, $PW_{12}O_{40}^{3-}$. The size of $PW_{12}O_{40}^{3-}$ is around 1.2 nm, which fits **EB-COF** pore size well. The nitrogen adsorption–desorption isotherms of **EB-COF:PW$_{12}$** showed extremely low values (8 m^2/g) suggesting POM anions occupying the pores of **EB-COF**. The C, H, and N and EDS elemental analysis of **EB-COF:PW$_{12}$** show that there are POM and Br ions in the channel (Table S2 and Figure S14). The elemental mapping of **EB-COF:PW$_{12}$** demonstrates elements P and W are homogeneously distributed throughout the whole pore structures (Figure S15). The **EB-COF** is stable after exchange in the acidic $H_3PW_{12}O_{40}$ solution, which was confirmed by PXRD (Figure S16).

To compare the difference of proton conductivity (σ) between **EB-COF:Br** and **EB-COF:PW$_{12}$** materials, ac impedance analysis was employed to evaluate the proton conductivities of **EB-COF:Br** and **EB-COF:PW$_{12}$**. The impedance analysis of two COFs was performed by using the corresponding compacted pellets of the powdered sample at 25 °C in the relative humidity ranging from 11% to 97%. According to the data of Nyquist plots at room temperature, the proton conductivity of the **EB-COF:Br** material ranges from 6.06×10^{-9} to 2.82×10^{-6} S cm^{-1} under RH 11% to 97%, which shows that the 1D porous channel facilitates water adsorption but the cationic COF framework alone cannot provide a continuous proton hopping pathway even at high relative humidity (Figure 3c and Figure S17). As comparison, POM anions were introduced into COF structure, and proton conductivity was measured (Figure 3d and Figure S18). With the increase of RH%, the proton conductivity value of **EB-COF:PW$_{12}$** continues to rise and reach 3.32×10^{-3} S cm^{-1} at 97% RH. From low RH (11%) to high RH (97%), the proton conductivity of **EB-COF:PW$_{12}$** is 100 times higher than that of **EB-COF:Br**, showing that the introduction of POM anions into pores of **EB-COF** greatly enhances proton conductivity of the material. To date, this is one of the best COF-based proton-conducting materials ever reported at room temperature. For example, the proton conductivities of PA@TpBpy-ST and PA@TpBpy-MC COFs at 393 K were reported to be 1.98×10^{-3} and 2.5×10^{-3} S cm^{-1}, respectively.[41b] Indeed, this value

DOI: 10.1021/jacs.5b13490
J. Am. Chem. Soc. 2016, 138, 5897–5903

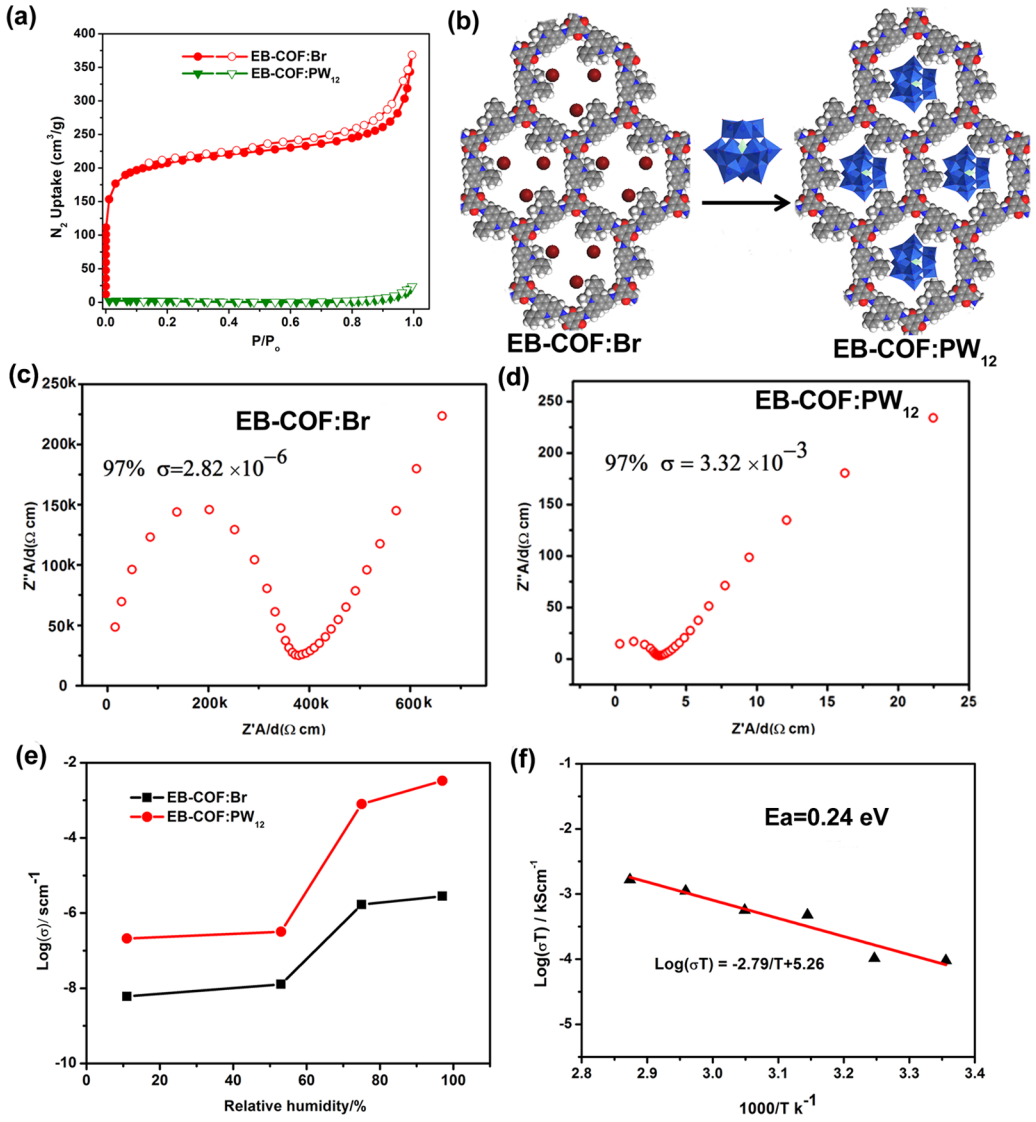

Figure 3. (a) Nitrogen sorption isotherms for **EB-COF:Br** and **EB-COF:PW$_{12}$**. (b) Schematic of $PW_{12}O_{40}^{3-}$ doping in COF. Proton conductivity of (c) **EB-COF:Br** and (d) **EB-COF:PW$_{12}$** in 97% RH condition. (e) RH dependence of the proton conductivity (σ) for **EB-COF:Br** and **EB-COF:PW$_{12}$** at 298 K. (f) Arrhenius-type plot of proton conductivity of **EB-COF:PW$_{12}$** at various temperatures under ~53% RH condition.

is comparable to those of several high-performing MOF materials, i.e., Fe-CAT-5 (5.0×10^{-2} S cm^{-1}),[42a] Fe(ox)$_2$H$_2$O (1.3×10^{-3} S cm^{-1}),[42b] and Ti-CAT-5 (8.2×10^{-4} S cm^{-1})[42a] under similar conditions (Table S3). To investigate the possible attribution of the surface effect on proton conductivity, we directly mixed COF with phosphotungstic acid and measured its conductivity. The observed proton conductivity of this mixed material was only 3.2×10^{-5} S cm^{-1} at 97% RH (Figure S19), which is much lower than that (3.32×10^{-3} S cm^{-1} at 97% RH) of **EB-COF:PW$_{12}$**. This result suggests that the contribution of surface conductivity is almost negligible.

It should be noted that dry **EB-COF:Br** pellets do not exhibit any notable proton conductivity under anhydrous condition. The direct current measurement also confirmed that the COF material is an electric insulator (Figure S20). A standard H_2/O_2 proton exchange membrane fuel cell test using a **EB-COF:PW$_{12}$** pellet as solid-state electrolytes showed a hydrogen pumping phenomenon demonstrating that the observed conductivity is protonic in nature (see Supporting Information for full details and Figure S21). We presumed that the hydrogen bond exchange between a keto-enamine group and the adsorbed H_2O can form H_3O^+, which acts as the proton source for proton conduction under humid conditions (Figures S22–S24). To support the proton conductivity mechanism, we conduct the conductivity measurement in deuterated water RH condition. The **EB-COF:Br** exhibited a proton conductivity of 9.8×10^{-7} and 1.32×10^{-6} S cm^{-1} at 75% RH (D_2O) and 97% RH (D_2O), respectively (Figure S25). These conductivities are nearly half those measured in water (1.7×10^{-6} and 2.82×10^{-6} S cm^{-1} at 75% RH and 97% RH, respectively). The decreased proton conductivity in deuterated water is caused by the isotopic effect of deuterium, whose mass is twice that of H atom. The isotopic effect supports our hypothesis that proton conduction across the **EB-COF:Br** is based on the transfer of protons derived from deprotonating adsorbed water in a humid environment. The increased proton conductivity of POM doped COF can be attributed to the formation of water clusters around $PW_{12}O_{40}^{3-}$ anions. Hydrophilic POM anions interacting with water molecules may provide interconnected hydrogen bonding networks with

DOI: 10.1021/jacs.5b13490
J. Am. Chem. Soc. 2016, 138, 5897−5903

in the 1D channel.[43] The good water retention ability of **EB-COF:PW$_{12}$** was also demonstrated by a water sorption isotherm at room temperature. As shown in Figure S25, **EB-COF:PW$_{12}$** exhibits significantly higher water uptake capacity than that of **EB-COF:Br** over the entire RH range measured, although **EB-COF:Br** has higher surface areas. The increase of proton conductivity of COF and **EB-COF:PW$_{12}$** with the increase of relative humidity suggests that the proton conductivity of the two materials is humidity-dependent. According to the Arrhenius plot, the E_a value of **EB-COF:PW$_{12}$** is 0.24 eV, which is comparable to that of Nafion film (0.21 eV).

CONCLUSION

In summary, we have successfully synthesized a cationic covalent organic framework **EB-COF:Br** with Br^- as counterions. This cationic framework shows high thermal and chemical stability and can be a simple platform for anionic exchange. Through ion exchange processes, a series of charged COFs (**EB-COF:X, X = F, Cl, Br, I**) have been prepared, and their porosity and pore sizes can be finely modulated. More importantly, by introducing polyoxometalates into this porous cationic framework, we can greatly enhance the proton conductivity of ionic COF-based material. The isotope-effect experiment and hydrogen pumping test proved the proton-conducting nature. **EB-COF:PW$_{12}$** shows the best proton conductivity at room temperature among reported COF materials. These properties suggest the cationic open COF framework can be an effective platform for ion exchange and proton conduction research. We believe that the ionic COFs are suitable for other ion (for example Li ion) conducting research in the near future.

ASSOCIATED CONTENT

Supporting Information

The Supporting Information is available free of charge on the ACS Publications website at DOI: 10.1021/jacs.5b13490.

Synthetic procedures and characterization details (PDF)

AUTHOR INFORMATION

Corresponding Authors

*lib020@ciomp.ac.cn

*zanghy100@nenu.edu.cn

Notes

The authors declare no competing financial interest.

ACKNOWLEDGMENTS

The authors gratefully acknowledge the financial support of the NSFC (Grant No. 21501166, 21471028, 51572256, and 51372240), National Kay Basic Research Program of China (No. 2013CB834802), and the Fundamental Research Funds for the Central Universities (No. 2412015KJ012).

REFERENCES

(1) Waller, P. J.; Gándara, F.; Yaghi, O. M. *Acc. Chem. Res.* **2015**, *48*, 3053.

(2) Slater, A. G.; Cooper, A. I. *Science* **2015**, *348*, 6238.

(3) Cote, A. P.; Benin, A. I.; Ockwig, N. W.; O' Keeffe, M.; Matzger, A. J.; Yaghi, O. M. *Science* **2005**, *310*, 1166.

(4) El-Kaderi, H. M.; Hunt, J. R.; Mendoza-Cortes, J. L.; Cote, A. P.; Taylor, R. E.; O' Keeffe, M.; Yaghi, O. M. *Science* **2007**, *316*, 268.

(5) Feng, X.; Ding, X. S.; Jiang, D. L. *Chem. Soc. Rev.* **2012**, *41*, 6010.

(6) Colson, J. W.; Dichtel, W. R. *Nat. Chem.* **2013**, *5*, 453−465.

(7) Doonan, C. J.; Tranchemontagne, D. J.; Glover, T. G.; Hunt, J. R.; Yaghi, O. M. *Nat. Chem.* **2010**, *2*, 235.

(8) Furukawa, H.; Yaghi, O. M. *J. Am. Chem. Soc.* **2009**, *131*, 8875.

(9) Ding, S. Y.; Gao, J.; Wang, Q.; Zhang, Y.; Song, W. G.; Su, C. Y.; Wang, W. *J. Am. Chem. Soc.* **2011**, *133*, 19816.

(10) Lin, S.; Diercks, C. S.; Zhang, Y.-B.; Kornienko, N.; Nichols, E. M.; Zhao, Y.; Paris, A. R.; Kim, D.; Yang, P.; Yaghi, O. M.; Chang, C. J. *Science* **2015**, *349*, 1208.

(11) Stegbauer, L.; Schwinghammer, K.; Lotsch, B. V. *Chem. Sci.* **2014**, *5*, 2789.

(12) Fang, Q.; Gu, S.; Zheng, J.; Zhuang, Z.; Qiu, S.; Yan, Y. *Angew. Chem., Int. Ed.* **2014**, *53*, 2878−2882.

(13) Colson, J. W.; Woll, A. R.; Mukherjee, A.; Levendorf, M. P.; Spitler, E. L.; Shields, V. B.; Spencer, M. G.; Park, J.; Dichtel, W. R. *Science* **2011**, *332*, 228.

(14) Wan, S.; Guo, J.; Kim, J.; Ihee, H.; Jiang, D. *Angew. Chem., Int. Ed.* **2008**, *47*, 8826.

(15) Bertrand, G. H. V.; Michaelis, V. K.; Ong, T.-C.; Griffin, R. G.; Dincă, M. *Proc. Natl. Acad. Sci. U. S. A.* **2013**, *110*, 4923.

(16) Dogru, M.; Handloser, M.; Auras, F.; Kunz, T.; Medina, D.; Hartschuh, A.; Knochel, P.; Bein, T. *Angew. Chem., Int. Ed.* **2013**, *52*, 2920.

(17) Calik, M.; Auras, F.; Salonen, L.; Bader, K.; Grill, I.; Handloser, M.; Medina, D.; Dogru, M.; Löbermann, F.; Trauner, D.; Hartschuh, A.; Bein, T. *J. Am. Chem. Soc.* **2014**, *136*, 17802.

(18) DeBlase, C. R.; Silberstein, K. E.; Truong, T. T.; Abruna, H. D.; Dichtel, W. R. *J. Am. Chem. Soc.* **2013**, *135*, 16821.

(19) DeBlase, C. R.; Hernandez-Burgos, K.; Silberstein, K. E.; Rodriguez-Calero, G. G.; Bisbey, R. P.; Abruna, H. D.; Dichtel, W. R. *ACS Nano* **2015**, *9*, 3178.

(20) Dalapati, S.; Jin, S.; Gao, J.; Xu, Y.; Nagai, A.; Jiang, D. *J. Am. Chem. Soc.* **2013**, *135*, 17310.

(21) Nagai, A.; Guo, Z.; Feng, X.; Jin, S.; Chen, X.; Ding, X.; Jiang, D. *Nat. Commun.* **2011**, *2*, 536.

(22) Tilford, R. W.; Mugavero, S. J.; Pellechia, P. J.; Lavigne, J. J. *Adv. Mater.* **2008**, *20*, 2741.

(23) Huang, N.; Krishna, R.; Jiang, D. *J. Am. Chem. Soc.* **2015**, *137*, 7079.

(24) Zeng, Y.; Zou, R.; Luo, Z.; Zhang, H.; Yao, X.; Ma, X.; Zou, R.; Zhao, Y. *J. Am. Chem. Soc.* **2015**, *137*, 1020.

(25) Zhu, Y.; Wan, S.; Jin, Y.; Zhang, W. *J. Am. Chem. Soc.* **2015**, *137*, 13772.

(26) Spitler, E. L.; Colson, J.; Uribe-Romo, F.; Woll, A.; Giovino, M. R.; Saldivar, A.; Dichtel, W. R. *Angew. Chem., Int. Ed.* **2012**, *51*, 2623.

(27) Fischer, S.; Schmidt, J.; Strauch, P.; Thomas, A. *Angew. Chem., Int. Ed.* **2013**, *52*, 12174.

(28) Yan, Z.; Yuan, Y.; Tian, Y.; Zhang, D.; Zhu, G. *Angew. Chem., Int. Ed.* **2015**, *54*, 12733.

(29) Yuan, Y.; Sun, F.; Li, L.; Cui, P.; Zhu, G. *Nat. Commun.* **2014**, *5*, 4260.

(30) Buyukcakir, O.; Je, S.; Choi, D.; Talapaneni, S.; Seo, Y.; Jung, Y.; Polychronopoulou, K.; Coskun, A. *Chem. Commun.* **2016**, *52*, 934.

(31) Van Humbeck, J. F.; Aubrey, M. L.; Alsbaiee, A.; Ameloot, R.; Coates, G. W.; Dichtel, W. R.; Long, J. R. *Chem. Sci.* **2015**, *6*, 5499.

(32) Mohanapriya, S.; Bhat, S. D.; Sahu, A. K.; Pitchumani, S.; Sridhar, P.; Shukla, A. K. *Energy Environ. Sci.* **2009**, *2*, 1210.

(33) Dou, W.; Zhu, L. Q.; Jiang, J.; Wan, Q. *Appl. Phys. Lett.* **2013**, *102*, 093509.

(34) (a) Ramaswamy, P.; Wong, N. E.; Shimizu, G. K. H. *Chem. Soc. Rev.* **2014**, *43*, 5913. (b) Yoon, M.; Suh, K.; Natarajan, S.; Kim, K. *Angew. Chem., Int. Ed.* **2013**, *52*, 2688. (c) Shimizu, G. K. H.; Taylor, J. M.; Kim, S. *Science* **2013**, *341*, 354.

(35) (a) Miras, H. N.; Vila-Nadal, L.; Cronin, L. *Chem. Soc. Rev.* **2014**, *43*, 5679. (b) Busche, C.; Vilà-Nadal, L.; Yan, J.; Miras, H.; Long, D.; Georgiev, V.; Asenov, A.; Pedersen, R.; Gadegaard, N.; Mirza, M.; Paul, D.; Poblet, J.; Cronin, L. *Nature* **2014**, *515*, 545.

(36) Katsoulis, D. E. *Chem. Rev.* **1998**, *98*, 359.

DOI: 10.1021/jacs.5b13490
J. Am. Chem. Soc. 2016, 138, 5897−5903

(37) Ramani, V.; Kunz, H. R.; Fenton, J. M. *Electrochim. Acta* **2005**, *50*, 1181.
(38) Saccà, A.; Carbone, A.; Pedicini, R.; Marrony, M.; Barrera, R.; Elomaa, M.; Passalacqua, E. *Fuel Cells* **2008**, *8*, 225.
(39) Kandambeth, S.; Mallick, A.; Lukose, B.; Mane, M.; Heine, T.; Banerjee, R. *J. Am. Chem. Soc.* **2012**, *134*, 19524.
(40) Contour, J. P.; Salesse, A.; Froment, M.; Garreau, M.; Thevenin, J.; Warin, D. *J. Microsc. Spectrosc. Electron.* **1979**, *4*, 483.
(41) (a) Chandra, S.; Kundu, T.; Kandambeth, S.; BabaRao, R.; Marathe, Y.; Kunjir, S.; Banerjee, R. *J. Am. Chem. Soc.* **2014**, *136*, 6570. (b) Shinde, D. B.; Aiyappa, H. B.; Bhadra, M.; Biswal, B. P.; Wadge, P.; Kandambeth, S.; Garai, B.; Kundu, T.; Kurungot, S.; Banerjee, R. *J. Mater. Chem. A* **2016**, *4*, 2682. (c) Ye, Y.; Zhang, L.; Peng, Q.; Wang, G.; Shen, Y.; Li, Z.; Wang, L.; Ma, X.; Chen, Q.; Zhang, Z.; Xiang, S. *J. Am. Chem. Soc.* **2015**, *137*, 913. (d) Xu, H.; Tao, S.; Jiang, D. *Nat. Mater.* **2016**, DOI: 10.1038/nmat4611.
(42) (a) Ponomareva, V. G.; Kovalenko, K. A.; Chupakhin, A. P.; Dybtsev, D. N.; Shutova, E. S.; Fedin, V. P. *J. Am. Chem. Soc.* **2012**, *134*, 15640. (b) Nguyen, N. T. T.; Furukawa, H.; Gándara, F.; Trickett, C. A.; Jeong, H.; Mo; Cordova, K. E.; Yaghi, O. M. *J. Am. Chem. Soc.* **2015**, *137*, 15394. (c) Yoon, M.; Suh, K.; Kim, H.; Kim, Y.; Selvapalam, N.; Kim, K. *Angew. Chem., Int. Ed.* **2011**, *50*, 7870. (d) Sadakiyo, M.; Yamada, T.; Kitagawa, H. *J. Am. Chem. Soc.* **2009**, *131*, 9906.
(43) (a) Amirinejad, M.; Madaeni, S. S.; Rafiee, E.; Amirinejad, S. *J. Membr. Sci.* **2011**, *377*, 89. (b) Okuhara, T. *Chem. Rev.* **2002**, *102*, 3641. (c) Liu, Y.; Sambasivarao, S. V.; Horan, J. L.; Yang, Y.; Maupin, C. M.; Herring, A. M. *J. Phys. Chem. C* **2014**, *118*, 854.

DOI: 10.1021/jacs.5b13490
J. Am. Chem. Soc. 2016, 138, 5897−5903